Nanoplastics on the coast exposed to the North Atlantic Gyre: Evidence and traceability

Mélanie Davranche[a], Caroline Lory[a], Corentin Le Juge[a], Florent Blancho[a], Aline Dia[a], Bruno Grassl[b], Hind El Hadri[b], Pierre-Yves Pascal[c], Julien Gigault[a,*]

[a] *Univ. Rennes, CNRS, Géosciences Rennes, UMR 6118, F35000 Rennes, France*
[b] *IPREM, UMR 5254, CNRS-Université de Pau et des Pays de l'Adour, F64000 Pau, France*
[c] *Institut de Systématique, Évolution, Biodiversité, UMR 7205, Université des Antilles et de la Guyane Française, Guadeloupe*

ARTICLE INFO

ABSTRACT

The occurrence of nanoplastics in the environment is now known and presents new threats linked to plastic debris issues. New questions about the formation pathways and life cycle assessment of nanoplastics in continental and marine environments have been raised. In the present study, we focused on the Guadeloupe island coastal system. For the first time, we demonstrated the presence of nanoplastics in sand water extracts (SWEs). We also investigated the potential of rare earth elements (REE) in tracing nanoplastics. Based on the REE patterns of SWEs, beached plastics and modern corals, we demonstrated that nanoplastics are important components in the REE signature of coastal sand (29 to 73%). These original results demonstrate the relevance of developing geochemical tracers for determining the fate of missing plastic litter.

1. Introduction

Plastic is ranked as the third most produced and manufactured material worldwide after cement and steel (Jambeck et al. 2015). The last estimations state that 8 Mt. of plastic were produced between 1950 and 2015, and 5 Mt. of plastic are estimated to be accumulated in landfills and natural environments(Geyer et al. 2017). Plastic pollution is now widely acknowledged. Rivers act as a major transport pathway for plastic debris into the seas (Schmidt et al. 2017), and then, the plastic debris accumulates into gyres(Colton et al. 1974; Howell et al. 2012), which drives and concentrates the plastics in oceanic regions. Up to 200,000 pieces of plastic per 1 km² are accumulated in these gyres. According to several studies and predictive models, hundreds of thousands of tons of plastics are floating on the surface of the oceans, which is 100 times less than the amount of plastics estimated to exist in the environment annually (Cózar et al. 2014; Jambeck et al. 2015). The reason for this gap remains unclear, but the scientific community converges on the degradation of plastics into nanometer-sized particles mainly under the action of light (photodegradation), oxidative conditions (thermo-oxidative degradation) (Andrady 2011), physical abrasion (Shim et al. 2014), and mechanical breakdown. Macroplastics (> 5 mm) are degraded into numerous micron-sized particles (Zbyszewski et al. 2014). From these plastic degradation pathways, we

recently demonstrated the continuous release of nanometer-sized plastics (Gigault et al. 2016). The nanoparticles of plastics, referred to as nanoplastics (NPs), are ranked from the 1 to 999 nm size range and/or present Brownian motion in aqueous systems (Gigault et al. 2018). According to the presence of organic matter or other colloidal materials present in the environment, NPs can agglomerate to form intermediate-sized particles between 1 μm and 100 nm.

However, the assumption of massive NPs occurring in our environment leads to many questions: are these NPs truly present in our systems? Where are the NPs? How exactly do the NPs form? What are the characteristics of NPs? At which level are we exposed to NPs? Compared to the presence of NPs in the North Atlantic Gyre (Ter Halle et al. 2017), a major question remains regarding their presence in coastal systems, and this represents considerable socioeconomic challenges, especially for those exposed to this massive vortex of plastic litter. Up to our knowledge there is no proof of their presence in such systems. The presence of NPs on coastal systems could also be explained by local source. Plastic debris can be released directly on coastal environment without passing through the oceanic circulation. Therefore, degradation of microplastics into nanoplastics can occurs in situ with a degradation pathways quite different to the one expected in marine environment.

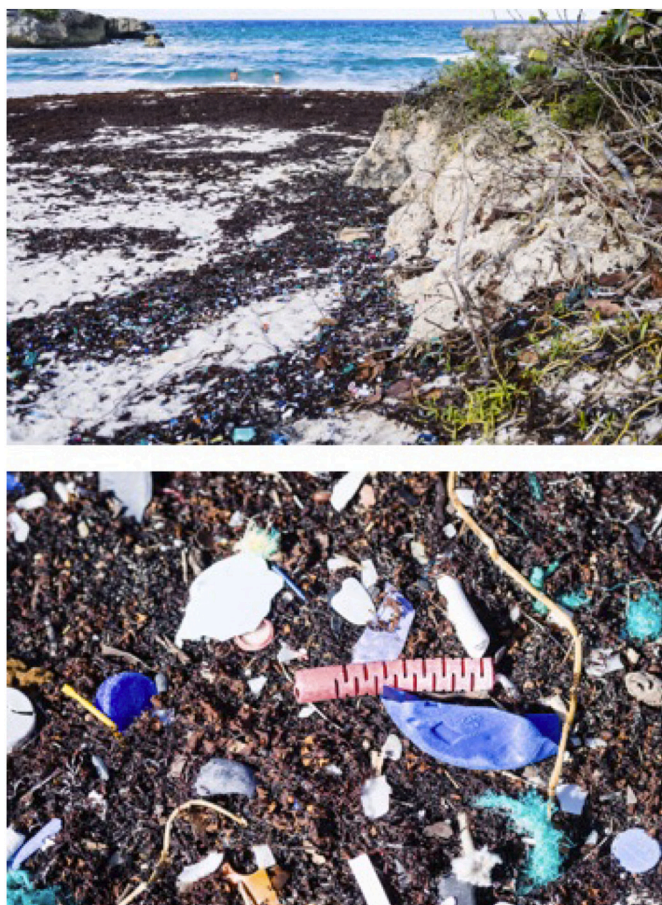Nanoplastics are expected to be nearly ubiquitous in the various

---

Fig. 1. Plastics deposited on Sainte Marie Beach (Guadeloupe, France). © Cyril Frésillon/Pepsea/CNRS library.

environmental compartments. However, there is lacks of proof since their analysis is still an open issues. There is a methodological gap for particles down to 1 μm (Schwaferts et al. 2019). Multi-analytical characterizations and quantification (Corti et al. 2020) as well as combinations of size fractionation-analytical technics were proposed (Fu et al. 2020; Schwaferts et al. 2019). Among all, this combination A4F-PyGCMS appear to be promising tool (Gigault et al. 2017; Mintenig et al. 2018; Wahl et al. 2021).

The main goal of the present work was to demonstrate the presence of NPs in coastal systems. As the study site, the French Guadeloupe island beach was chosen due to its exposure to the North Atlantic Gyre. The oceanic current and hurricanes that pass through the tropical zone represent a source of plastic litter on beaches. We inventoried different coasts of Guadeloupe island (*Grande Terre*) to evaluate the degree of plastic presence and the position of plastics relative to the NOA gyre. The chosen beach was largely covered in macroplastic and microplastic debris (Fig. 1).

We developed an experimental setup that associated a NPs extraction protocol with a multi-characterization approach dedicated to nanometer-sized species by focusing on size and chemical composition; this approach included geochemical tracers, such as rare earth elements

(REE). As with other nanoscale and colloidal materials, the main properties of NPs are their large surface area and their high mobility. As a consequence, colloidal materials can significantly concentrate more chemical elements (trace metal and organic molecules) on their surface than their micron-sized analogues. Several studies have already demonstrated that microplastics collected in the Atlantic gyre contain significant amounts of metals (As, Fe, Cd, Pb, etc.) that are adsorbed and/or present due to plastic formulation (Brennecke et al. 2016; Prunier et al. 2018). Other studies highlighted that the aged polymer pellets collected on beaches are more likely to adsorb contaminants, such as metals, than new plastic pellets (Holmes et al. 2012). Aged plastic thus appears to be a carrier of metals, offering an opportunity to trace and track their environmental fate and impact. Here, we focused on rare earth elements. We tested the ability of the REE pattern to evaluate the NPs contribution to the REE signature and the potential of REE to be used as nanoplastic tracers.

2. Materials and methods

2.1. Samples

The studied samples were collected from the beach of the Bay Sainte-Marie (*Grande Terre*, Guadeloupe, France), which is exposed to the North Atlantic gyre and known to be widely contaminated by plastic debris. *Grande Terre* island is a calcareous island constituted by a low coralline terrace that was shaped during the Eemian (Battistini and Hinschberger 1985). Plastics were collected directly from the beach using a net of 100 nm mesh. The chemical composition of the bulk sand sample (plastics and sand) was determined at the Service d'Analyse des Roches et des Minéraux (SARM, France). After fusion of the sample with $LiBO_2$ and acid digestion with HNO_3, the major elements were determined by inductively coupled plasma-optical emission spectrometry (ICP-OES; iCap6500 ThermoFisher), and the trace elements were measured by inductively coupled plasma-mass spectrometry (ICP-MS; iCapQ ThermoFisher) (Table 1).

2.2. Sand water extraction experiments

The NPs were extracted from the sand sample with ultrapure water at a 1:4 sand/water ratio in 500 mL total volume at a natural pH (measured equal to 8.5). The suspension was stirred for 64 h until the DOC concentration reached equilibrium, and then it was filtered at 5 μm to remove the major, macro- and microscale-sized particles. The < 5 μm fraction was subsequently filtered at 0.8 and 0.2 μm (Sartorius). All of the sand water extraction (SWE) experiments were performed in triplicate. Blank experiments were carried out to determine possible contaminations, which were always negligible.

2.3. Size determination and elemental characterization

The particle size was determined by differential light scattering (DLS) using a VASCO Flex™ (Cordouan Technologies). The probe was placed in front of the glass vial and measured directly in the water extract. Each measurement is a statistical average of six measurements, each composed of six acquisitions of light scattering for 120 s. The data were processed with NanoQ™ software. The detection of Brownian motion particles is directly related to their hydrodynamic size at a

Table 1
Geochemical composition of the sand sample.

%											ppb
SiO_2	Al_2O_3	Fe_2O_3	MnO	MgO	CaO	Na_2O	K_2O	TiO_2	P_2O_5	Fire Loss	ΣREE
0.49	0.13	0.06	0.003	3.39	51.65	0.14	0.01	0.007	0.050	43.88	3.08

known viscosity and temperature. The colloidal size distribution ranged from 1 to 1000 nm. Autocorrelation curves obtained by DLS of the different fractions are characteristic of a Brownian motion with an exponential decreasing curve that shows the presence of nanoparticles in solution. The hydrodynamic diameter Z-average (d_{zH}) from the ACF algorithm function (Cumulants) corresponds to the harmonic mean of the particles based on the scattered light intensity (DLS).

2.4. Transmission electron microscopy (TEM) observations

Before TEM analysis, SWE solution was purified to remove excess of salt and concentrated using a Xpress micro-dialyzer system (Scienova, Germany). A drop of the solution was deposited onto a 300-mesh copper grid coated with a lacey carbon film (Oxford Instruments, S166–3) and dried at room temperature. High-resolution electron microscopy (HREM) investigations were performed on a TEM with a JEOL 100CXII instrument (voltage 100 kV) (THEMIS Analytical Facility at the University of Rennes 1). The elemental composition of the different structures was determined with a JEOL 2100F (voltage 200 kV) equipped with an X-ray energy dispersive spectroscopy (XEDS) detector (Kevex detector with an ultrathin window).

2.5. Presence of plastics and their composition determination

Pyrolysis GC–MS (Py-GCMS) was conducted with a 3030D Multi-Shot pyrolizer (Frontier Lab, Japan) coupled to a 5977B gas chromatography–mass spectrometry setup (Agilent Technology, SRA, France). Pyrolysis was performed at 700 °C for 1 min. For GC molecule separation, the helium gas flow was set at 1 mL min^{-1} and the temperature ramp was set at 50 °C for 2 min, then set at 15 °C min-1 until 180 °C was reached and finally set at 5 °C min-1 until 310 °C was reached. Ionization was carried out by an electronic impact at 70 eV, and the ion source and the interface were heated at 200 °C and 280 °C, respectively. Mass spectra detection was performed in a full scan for all m/z ranges between 50 and 600. According to the literature and to Table S1 (which is a list of plastic molecular markers by Py-GCMS), the standard chromatograms of nanoscale PE, PET, PVC, PP and PS were also analyzed. Such standards were prepared as previously described (El Hadri et al. 2020). For the analysis, 50 μL of SWE solution was placed in a glass cup and dried at 60 °C. Then, the cup was placed into the pyrolizer. Each chromatogram was repeated 3 to 6 times.

2.6. Major and trace elemental analysis

The major and trace elements, including the REE, were measured using a Quadrupole ICP-MS (Agilent Technologies 7700×). The concentrations were determined using a conventional external calibration procedure with multi-elemental solutions acidified to 2% in HNO$_3$, and a rhodium solution was used as an internal standard to correct the instrumental drift and potential matrix effects. The limit of detection for all the groups of REE was between 0.0003 and 0.0006 ppb, and the REE chemical blanks were below the limit of detection and are thus negligible. The analytical method required a mineralization step for the OM-rich solutions (DOC > 20 ppm), mainly for fractions < 5 and < 0.8 μm, to avoid interferences with the organic carbon mass analysis by ICP-MS. The solutions were digested with nitric acid (14 N HNO$_3$) at 100 °C for 24 h, and after complete evaporation, the residue was solubilized in 0.37 N HNO3.

2.7. Ce and Eu anomaly calculation

The cerium anomaly (Ce*) can be quantified using the following equation:

$$Ce* = 2Ce_N/(La_N + Pr_N^1) \tag{1}$$

(^{1} or Nd_N when compared to the average modern coral REE pattern, since the Pr concentration was not available, the corresponding Ce anomaly was noted $Ce*_{Nd}$)

The Eu anomaly (Eu*) was quantified using:

$$Eu* = 2Eu_N/(Sm_N + Gd_N) \tag{2}$$

with $_N$ corresponding to the PAAS normalized abundance.

3. Results & discussion

3.1. Evidence of nanoplastics on the Guadeloupian coast

The beach sand samples were collected on the beach of the Bay *Sainte-Marie* (Guadeloupe, France) in *Grande Terre* Island, which is exposed to the North Atlantic gyre (NAG); this area is known to be widely contaminated by plastic debris (Fig. 1). To examine the presence of NPs in the beach sand, an ultrapure water extraction method was applied to the sand sample. At equilibrium, the suspension was filtered at 5 μm to remove the major and macro- and microscale-sized particles and was subsequently filtered at 0.8 and 0.2 μm to classify the NPs and colloidal materials. For the different sand extraction filtration cutoffs, we performed size analysis using dynamic light scattering (DLS) analysis. According to DLS theory, the autocorrelation (characterized by an exponential decay) of the light intensity scattered with time indicates the presence of colloidal materials (Fig. 2).

The difference in the decrease in the exponential decay between the < 5 μm fraction and the < 0.8 μm and < 0.2 μm fractions indicates a large size distribution (d_{zH} of 1974 ± 152 nm for the < 5 μm fraction), with the rate order in the exponential decay following the filtration cutoff. The < 0.8 and < 0.2 μm fractions presented similar variations, showing a slight decrease in d_{zH} from 551 ± 45 nm to 370 ± 31 nm, respectively. After 3400 μs, the < 0.8 and < 0.2 μm fraction signals were noisy and passed the 5 μm cut-offs, which is characteristic of large noncolloidal particles (μm-scale) at low concentrations. For all the fractions, dissolved organic carbon (DOC) was quite constant at approximately 3 mg L^{-1}, indicating that all the
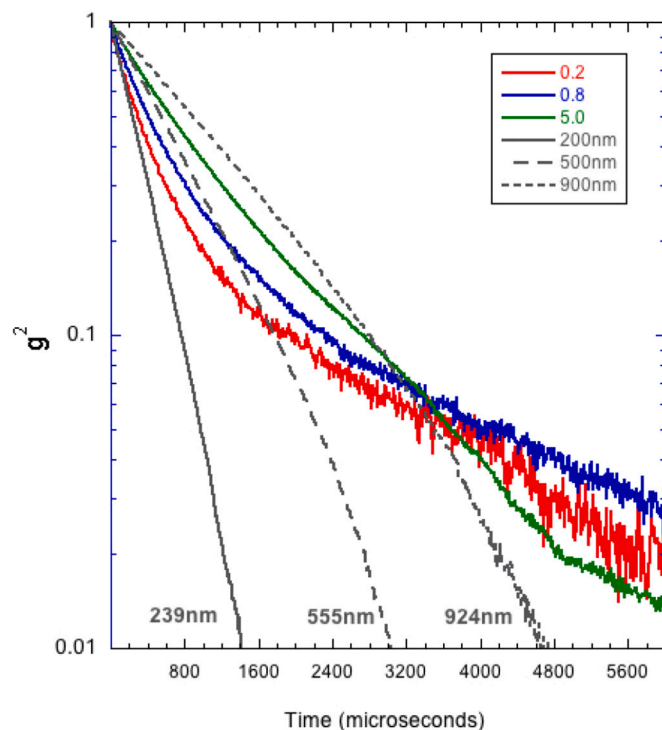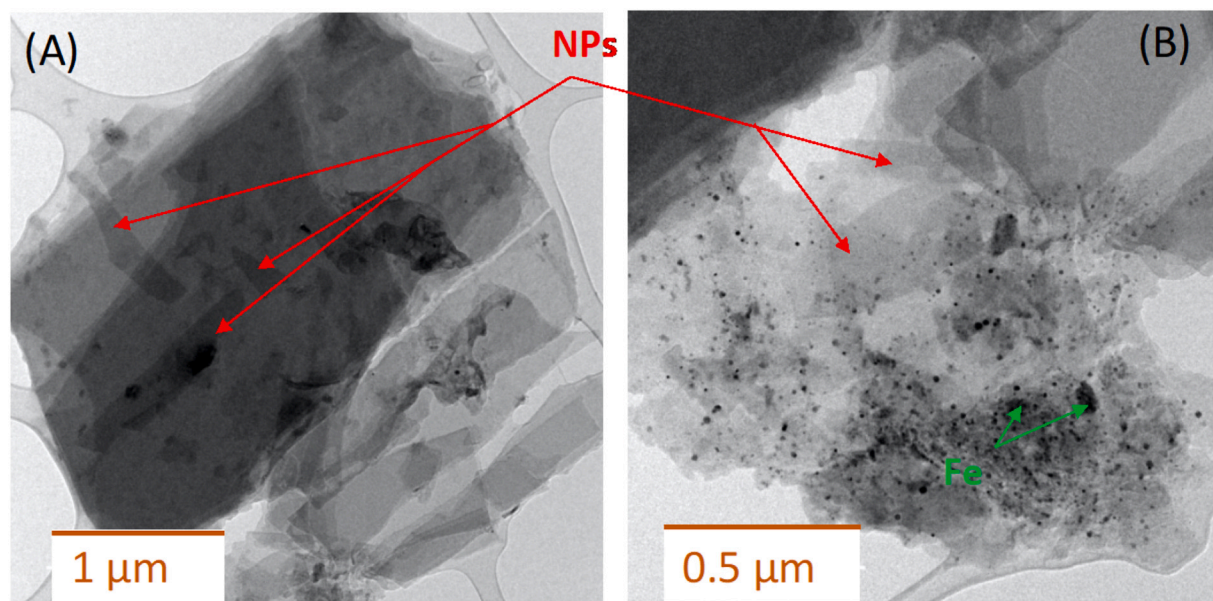

Fig. 2. Autocorrelation curves and the corresponding Z average value, obtained by DLS, from each filtration of the sand samples.

Fig. 3. Transmission electron microscopy (TEM) images of the SWE. (A) Large carbon particles that degrade into smaller ones (from 200 to 1000 nm), (B) Red arrow show nanoparticles which composition, size and shape suggest to be NPs, dark dots show by green arrows correspond to Fe nanoparticles. (For interpretation of the references to color in this figure legend, the reader is referred to the web version of this article.)

organic matter (OM), including NPs, was located in the colloidal size range (1–1000 nm) (SI, Fig. S1). However, knowing the asymmetrical and polymorphic structures of NPs and colloidal OM, the filtration cutoff cannot be used as a size evaluator. A slight increase in the dissolved inorganic carbon (DIC) from 15 to 17 mg L^{-1} (materials and methods section) was observed between the < 0.2 μm to < 5 μm fractions that could be caused by the dissolved carbonate particles that can possibly interfere with the DLS measurement.

Transmission electronic microscopy (TEM) was performed on the SWE. Nanoparticles with size ranging from 200 to 1000 nm were observed (Fig. 3). Analyses by EDX showed the absence of Ca and a net positive carbon contrast between nanoparticles and amorphous carbon of the TEM grid (SI, Fig. S2). The focus of the electron beam at higher tension did not involve modifications suggesting a high stability of the nanoparticles. The carbon composition, size, shape and stability suggest thus NPs. Fig. 3 show also the presence of small Fe nanoparticles varying from 1 to 30 nm as dark spherical spots (Fig. 3B).

Even if TEM and DLS suggest the presence of NPs, all these techniques are not selective for NPs. For this reason, pyrolysis coupled to gas chromatography and mass spectrometry (Py-GCMS) was used to identify the presence of plastics associated with the size distribution (Ter Halle et al. 2017). As summarized in the supplementary information (SI-Table S1), during pyrolysis at high temperature (i.e., > 600 °C), each plastic releases a specific pattern of molecules (Kusch 2012). However, some of these molecules are biochemical markers of natural biomass (vegetation and algae), such as benzene, toluene, styrene, and naphthalene. To investigate and distinguish the NPs (generally diluted) signature within the sand matrices, different "standards" were used: (i) polystyrene and polyvinyl chloride nanoparticles produced as described in (El Hadri et al. 2020) and (ii) a Sargassum algae water extract (SaWE). Massive amounts of Sargassum algae are transported from the NOA to the Guadeloupean beaches and exposed to the gyre, and they are generally mixed with plastic (Fig. 1). We sampled Sargassum algae without any surrounding plastics. For the sand samples, water extraction was performed from the algae. This water extract is representative of the OM quality present in the sand water extracts (SWE).

Fig. 4 illustrates the chromatogram for the SaWE in the < 0.8 μm fraction. The chromatograms for the PS-NP and PVC-NP models are presented in the supplementary information (SI, S2-Fig. S2). Compared
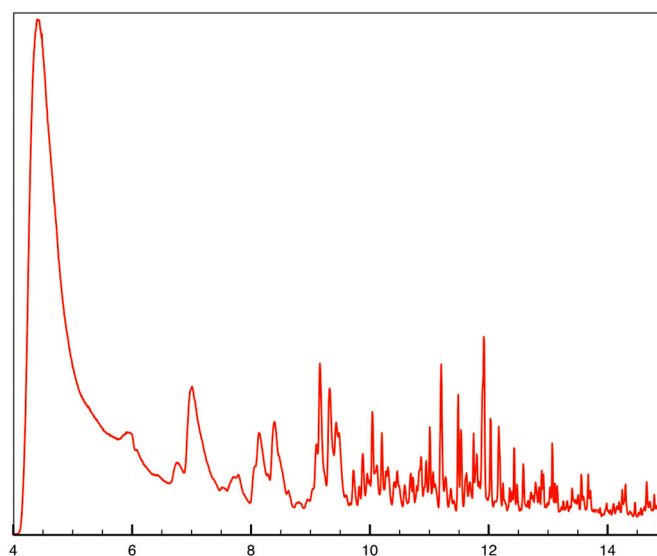
Fig. 4. Total ion chromatogram obtained for the < 0.8 μm fractions of the SWE and the Sargassum water extract (SaWE).

to the models, benzene (Benz), toluene (Tol), styrene (Sty), indene (Ind), naphthalene (Nap), and methylnaphthalene (M-Nap) were easily identified. These markers suggest the presence of PVC and PS. To determine and validate the contribution of plastics from the OM signal, the ratio of specific markers was used.

Table 2 summarizes the ratios for PVC, PS, SaWE and SWE fraction < 0.8 μm. Because Nap is the most predominant marker for PVC, it was chosen to calculate the ratio with the other PVC markers. Compared to SaWE, the SWE fraction < 0.8 μm presented X/Nap ratios (X corresponds to the marker summarized in the table) closest to that of the PVC-NP, except for styrene. The deviation in the Sty/Nap ratio from PVC-NP below the SaWE value suggests a contribution of a Sty other than OM, and it is probably from polystyrene NPs. The Tol/Sty ratio is known to be an appropriate indicator of OM contribution to the polystyrene signal by Py-GCMS (Fabbri et al. 1998; Watteau et al. 2018). A net difference between the PS-NP and PVC-NP Tol/Sty ratio (≈ 0.15)

Table 2
Molecular ratio of the main plastics and natural organic matter pyrolysis products for PVC-NP and PS-NP.

		Tol/Nap	Benz/Nap	Sty/Nap	M-Nap/Nap	Tol/Sty
Standards	PVC (10–500 nm)	0.64 ± 0.02	2.2 ± 0.2	3.85 ± 0.32	0.04 ± 0.01	0.16
	PS (200–400 nm)					0.012 ± 0.002
	SaWE	6.6 ± 0.4	*	1.33 ± 0.06	0.37 ± 0.02	4.9 ± 0.1
SWE	< 0.8 μm	0.9 ± 0.01	1.44 ± 0.05	0.57 ± 0.01	0.12 ± 0.01	1.55 ± 0.2

and OM (≈ 5) was observed. A Tol/Sty ratio of 1.55 is obtained for the SWE fraction < 0.8 μm. In the literature, OM generally presents a Tol/Sty ratio > 5, and a Tol/Sty ratio ranging from 0 to 1 is characteristic of polystyrene plastic (Fabbri et al. 1998). The higher Tol/Sty ratio of the SWE fraction < 0.8 μm compared to PS-NP can be explained by OM, as observed for the PVC. In a soil amended with plastic wastes, Watteau et al. recently determined the Tol/Sty ratio for the 0–2 μm soil fraction, and the Tol/Sty ratio ≈ 3 compared to a Tol/Sty ratio ≈ 5 for a non-amended fraction (Watteau et al. 2018). In another study, we obtained a similar Tol/Sty ratio ≈ 2–3 for NPs of polystyrene in landfill soil (Wahl et al. 2020). Compared to the beaches, the soil system contains generally higher OM concentrations. Considering the surface properties of NPs, they naturally heteroaggregate with such OM. Therefore, the mass contribution of OM to the plastic increases significantly with decreasing particle size. The present results indicate the presence of PS and PVC in the colloidal fraction of the SWE with a low OM contribution, which is logical considering the solution color.

Finally, polypropylene was not identified, and its principal marker (2,4-dimethyl-1-heptene) was not detected. Nevertheless, the chromatogram of the SWE with a fraction < 0.8 μm shows the presence of aliphatic compounds (Fig. 5).

These compounds are composed of linear hydrocarbons (m/z 55 and 57) with one or two unsaturated carbons (C11 to C18), which is characteristic of PE. Generally, as demonstrated by Ter Halle et al., a triplet of n-alkadiene, n-alkene and n-alkane with a bimodal distribution is characteristic of the molecular PE formation pathways during pyrolysis compared to OM (Ter Halle et al. 2017). However, due to the contribution of OM to the signal and the low PE amount regarding the detection limit of the Py-GCMS, their relative abundance makes their identification difficult to achieve. To validate the presence of PE, the ratio between alkene and toluene was investigated, since toluene is one of the main pyrolysis products.

Table 3 presents the toluene/alkene (Tol/Alk) ratio for the SaWE and SWE. The SWE Tol/Alk ratios are lower than those of the SaWE Tol/Alk ratios, indicating lower toluene or higher alkene concentrations. This difference can either be caused by a lower OM amount or a contribution of PE to the alkene signals. Nevertheless, if only OM contributed to the alkene signal, the Tol/Alk ratio should be quite constant; however, this is not the case here. Moreover, even if these aromatic and aliphatic compounds were detected in the SWE, pyridines, amines and indoles (Biller and Ross 2014; Dignac et al. 2005; Rouches et al. 2017) were not detected in our samples, which confirms the
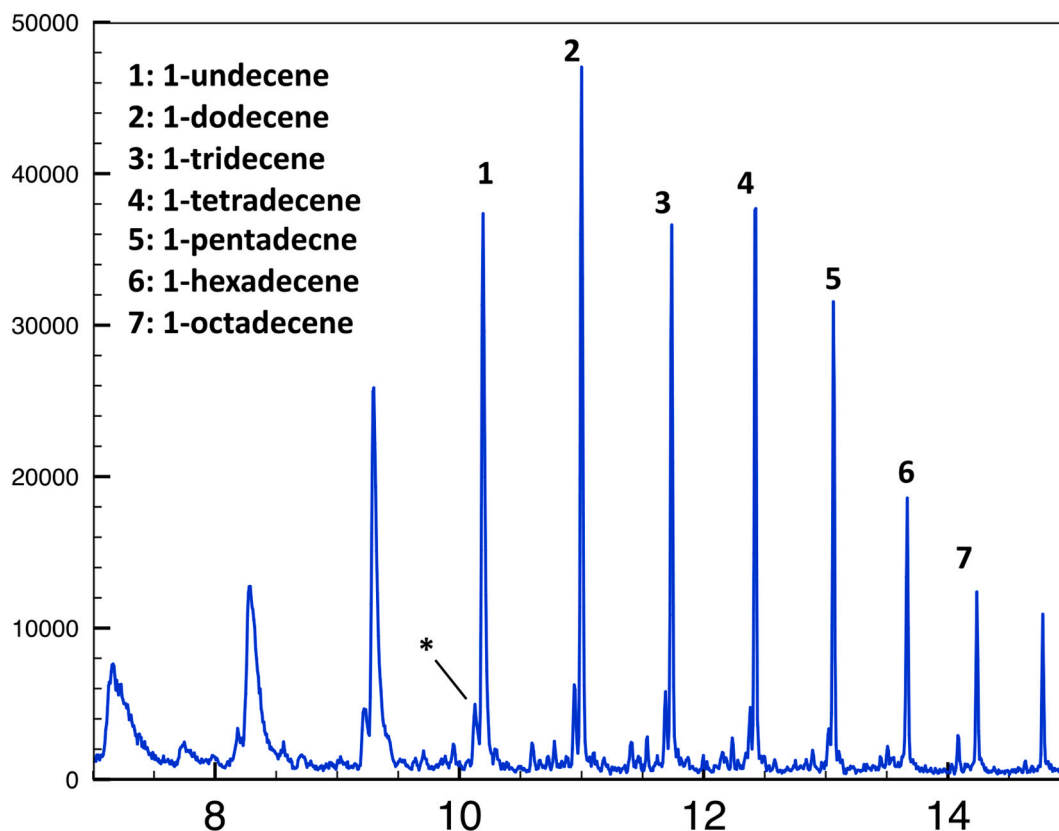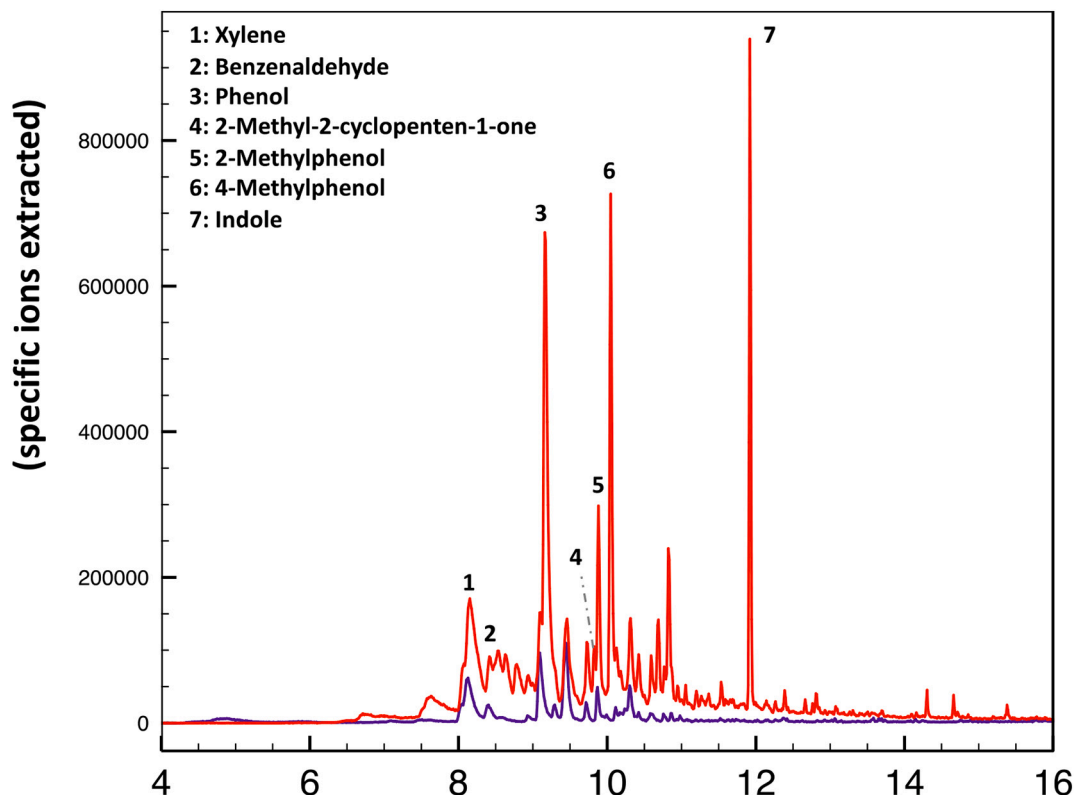

Fig. 5. Specific ion chromatogram of molecules listed (1–7) for the < 0.8 μm fractions of the SWE and the Sargassum water extract (SaWE). *Presence of the Alkadiene.

Table 3
Molecular ratio of toluene to alkene for the SaWE and SWE fractions < 0.8 μm.

Toluene/X	1-Undecene	1-Dodecene	1-Tridecene	1-Tetradecene	1-Pentadecene	1-Hexadecene	1-Octadecene
SaWE	77.7 ± 6.7	98.1 ± 8.2	77.9 ± 14.0	88.1 ± 3.6	70.3 ± 10.5	131.9 ± 21.8	228.8 ± 51.2
SWE < 0.8 μm	50.2 ± 4.3	45.7 ± 3.9	53.8 ± 4.7	50.7 ± 4.4	58.7 ± 7.4	99.4 ± 8.3	147.2 ± 11.2

Fig. 6. Specific ion chromatogram of molecules listed (1–7) for the < 0.8 μm fractions of the SWE and the Sargassum water extract (SaWE).

presence of PE in the NPs composition.

Finally, to characterize the natural OM associated with NPs, we investigated the major ions identified in the SaWE except for toluene, benzene, styrene, and naphthalene, as these compounds can be assimilated to PS and PVC. Fig. 6 presents the SWE and SaWE chromatograms with the principle identified ions: xylene; benzenaldehyde; phenol; 2-methylphenol; 4-methylphenol; indole; and 2-methyl-2-cyclopenten-1-one. Indole was selected to represent the protein fraction (Biller and Ross 2014), while 2-methyl-2-cyclopenten-1-one is a reliable marker of polysaccharides and carbohydrates (Dignac et al. 2005; Rouches et al. 2017). A net difference occurs between both solutions, confirming the contribution of PS and PVC NPs to the signal. However, as expected, similarities between the SWE and SaWE appear, suggesting a contribution of the Sargassum algae to the nanoplastic signal, which is consistent with the sampling area. There was no indole detected in the SWE, suggesting that the OM associated with the NPs are not proteins. Regarding the sampling site conditions (sand, UV, and temperature), protein-like molecules are rapidly degraded. Therefore, the natural OM associated with NPs of PS and PVC are essentially aromatic.

3.2. Traceability of nanoplastics

Although the identification of the presence of NPs in the environment is challenging, their source and fate are essential to accurately determine their impact and to propose adequate regulation. To address this challenge, we were interested in the rare earth elements (REE)

chemical group in regards to their ability to trace sources and biogeochemical processes. Rare earth elements, or lanthanides, constitute a group of elements with coherent chemical properties. The tracing properties of REE correspond to small observable variations within the group that occur according to the environmental conditions (sources, pH, Eh, ligands, biogeochemical processes, etc.). Such variations, named REE fractionations, are observable in the REE patterns that correspond to the evolution of their relative abundance with their increasing atomic numbers, normalized to their amounts in the crust (McLennan 1989). Various normalizations are used; here, we chose the PAAS (Post Australian Archean Shale) (McLennan 1989) according to the coral origin of the collected sand (Battistini and Hinschberger 1985). To evaluate the potential traceability of NPs by REE, we studied the REE patterns of the SWE < 0.8 μm fraction (Fig. 7A).

Note that the redox behavior of Ce and Eu is revealed in the REE pattern by a positive or negative anomaly (McLennan 1989). The REE pattern of the SWE < 0.8 μm fraction was concave with a negative Ce anomaly (Ce* = 0.60) and by a slight enrichment in heavy REE (HREE) as revealed by the La/Lu ratio = 0.77 and the Gd/Yb ratio = 1.5. A slightly positive Eu anomaly (Eu * = 1.10) and a middle REE (MREE) concavity (so-called MREE downward concavity) were also developed on the REE pattern. This MREE downward concavity is attributed to the REE binding with the carboxylic sites of the OM or with the OH sites of the Fe and Mn oxyhydroxides (Bau 1999; Davranche et al. 2015). Dissolved organic carbon (DOC) was, however, mainly composed of small organic molecules with sizes < 0.2 μm, while there were 93% REE in

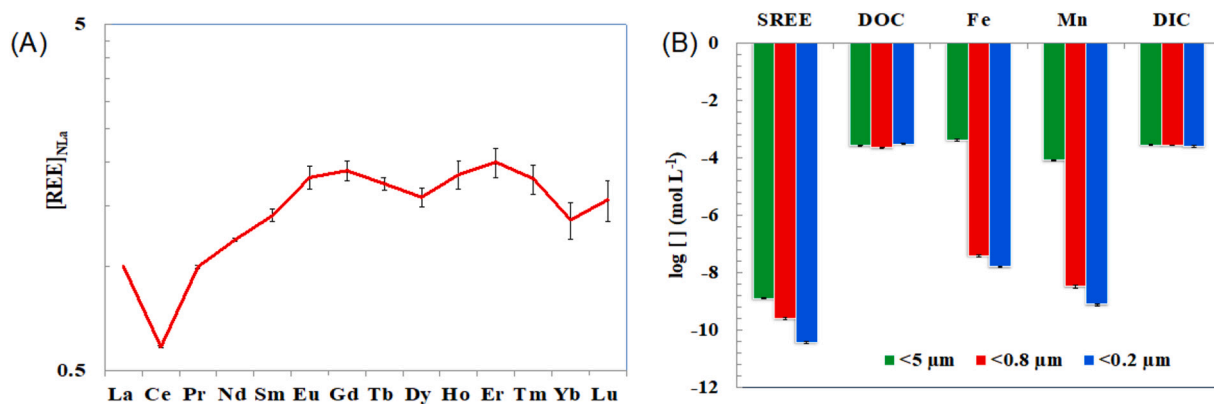**Fig. 7.** A) PAAS and La normalized REE patterns of the SWE < 0.8 μm fraction, and B) ΣREE, DOC, FE, Mn and DIC concentrations in each fraction (log mol L^{-1}). Error bars correspond to triplicate extraction experiments.

the fraction > 0.2 μm (Fig. 7B), suggesting that OM was not the major origin of REE in the SWE < 0.8 μm fraction. Although Fe and Mn were more concentrated in the < 5 μm fraction as particulate Fe/Mn oxyhydroxides (Fig. 3), their concentrations in the SWE < 0.8 μm fraction were sufficient to significantly complex REE. However, the MREE downward concavity developed in response to the REE binding to the Fe and Mn oxyhydroxides presents a binding maximum for Sm (Bau 1999; Pourret et al. 2007). The binding maximum obtained here for Eu and Gd suggested that Fe/Mn oxyhydroxides were not the major binding phases of REE. The coral source of sand associated with the high DIC concentration should involve a net enrichment in the HREE as observed in the REE patterns of coral carbonates (Sholkovitz and Shen 1995) (Fig. 7B). The REE pattern of the SWE < 0.8 μm fraction suggests that REE could be bound or carried by another phase. Since NPs were easily detected in this fraction and are able to bind metals (Davranche et al. 2019) and REE as demonstrated elsewhere (SI, Fig. S4), we can clearly hypothesize that the REE pattern could be the result of coral sand dissolution and the presence of REE-bearing NPs.

To test and validate this hypothesis, the REE pattern of the SWE < 0.8 μm fraction was compared to the REE patterns obtained from the acidic digestion of beached microplastics that were collected on the Guadeloupe island beach and to the REE pattern of a modern coral sand (Sholkovitz and Shen 1995) (Fig. 8). Note that the coral terraces of *Grande Terre* belong to massive coral species, such as *Asteroid, Favia, Diploria, Montastrea* and *Siderastrea* (Battistini and Hinschberger 1985). Therefore, the reference REE pattern of the modern corals corresponds to the average of the REE patterns determined for each of these species (Sholkovitz and Shen 1995). Moreover, to allow comparison and because the exact concentrations of REE in each source were not known, all REE patterns were normalized to La. The REE pattern of the beached plastics was slightly depleted in the HREE with La/Lu = 1.35 and Gd/Yb = 1.40, and no Ce anomaly was observed (Ce*Nd = 0.53). The only characteristic feature was the development of a marked positive Eu anomaly (Eu* = 3). Two possibilities can explain this anomaly: (i) Europium was present as an additive in plastics (Maris et al. 2012), or (ii) the Eu mass (m/z) interference by

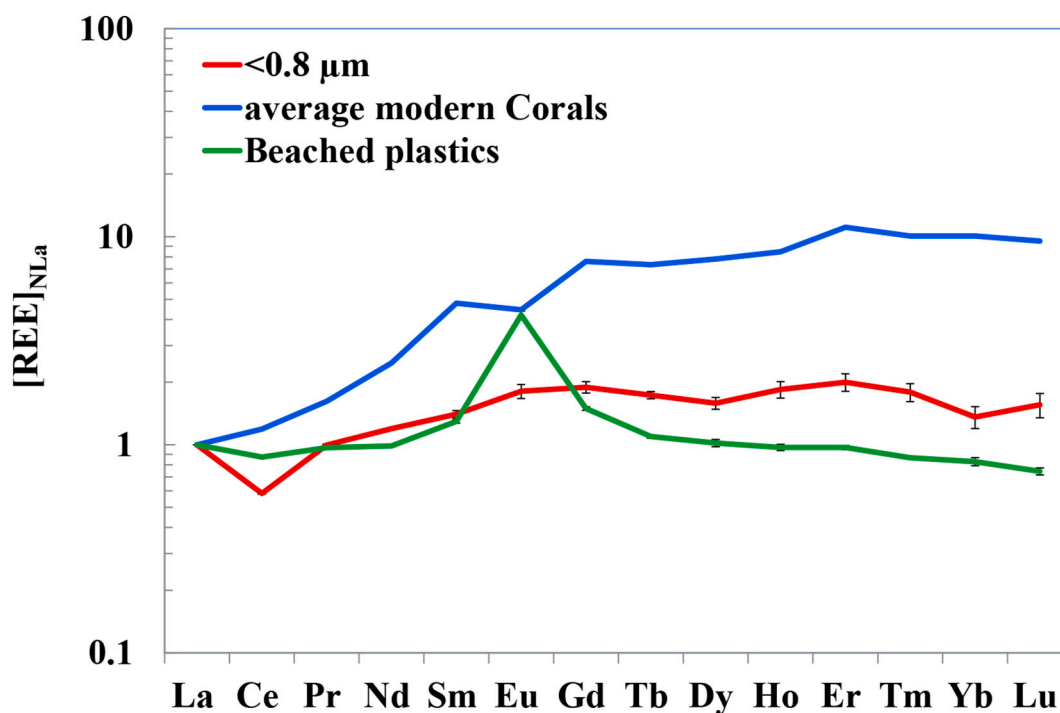**Fig. 8.** Comparison of the normalized (PAAS and La) REE patterns of the < 0.8 μm fraction with the REE patterns of the average modern corals *(23)* and the beached plastics.

Ba occurred during the ICP-MS measurements. Above a certain concentration, Ba starts forming oxides and hydroxides during ICP-MS analysis, which creates isobaric interferences with Eu (Nelms 2009). Note that Ba is a current additive in plastics (Maris et al. 2012). To investigate these possibilities, we first measured the Ba concentrations in the beached plastics to be 1.8 ± 0.2 mg kg^{-1}. The possible Ba interference could be mathematically corrected using the Ba standards for low Eu/Ba ratios. Different Ba standard concentrations were thus tested, allowing to conclude that the positive Eu anomaly (Eu* = 1.26) on the digested beached plastics was inherent to the Eu concentrations and not inherent to the Ba interferences. The Eu anomaly can thereby be attributed to a NPs contribution.

The REE pattern of the average modern corals exhibits negative Eu and Ce anomalies (Eu* = 0.62 and Ce*$_{Nd}$ = 0.68) (Fig. 7). This REE pattern also displayed a continuous enrichment from La to Lu, as expected for carbonate REE-bearing phases with La/Lu = 0.09 and Gd/Yb = 0.75. The REE pattern of the average modern corals and the NPs-enriched SWE < 0.8 μm fraction were therefore both enriched in HREE as compared to the digested beached plastics, which was confirmed by the La/Lu and Gd/Yb ratios. However, surprisingly, the Ce anomaly was the highest for the SWE < 0.8 μm fraction. Therefore, regarding the continental environment of the beach, we cannot exclude that particulate Mn and/or Fe oxyhydroxides present in the sand were preferentially sorbed and oxidized Ce (Bau 1999; Ohta and Kawabe 2001). The REE pattern of the SWE < 0.8 μm fraction could be due to a mixing of the REE-bearing corals sand and REE-bearing NPs.

Based on this result, we used the Eu anomaly and the La/Sm and Gd/Yb ratios to evaluate the proportion of each phase. The Ce anomaly was discarded because it cannot be attributed to the coral sand or to the NPs. We used a mixing equation with coral sand and beached plastics as both extremes. If the calculation did not provide conclusions about the dominant REE-bearing phase (Table 4), then they provided evidence that NPs were of major importance in the REE amount and pattern development, since calculations showed that their proportions could vary between 29 and 73% (Table 4).

These results could be refined by determining the exact REE pattern of the coral sand. However, these data are probably impossible to obtain, since the whole *Grande Terre* coast that is exposed to the NAG is impacted by plastic deposits. These results demonstrate that REE could be interesting tracers to examine and potentially quantitatively evaluate the presence of NPs in continental environments that result from plastic deposits (such as ancient landfills and plastic mulched soils). The major limit of the REE tracer is the REE concentration in NPs that depends not only on the REE affinity for NPs but also on the plastic formulation (e.g., Eu as plastic additives). However, regarding the strong alteration degree of nanoplastics, only REE as additive used in high concentration is expected to be conserved in NPs. Moreover, an individual or a combination of specific REE are generally used in plastics formulation to enhance specific properties (Balaram 2019), while in the environment, the whole group of REE is present. Both points are extremely interesting for the tracing properties of REE. Indeed, if one REE is associated to NPs, it will be present at relative larger amount compared to the others (El Hadri et al. 2021). Therefore, a anomaly specific to this REE and then to the plastics is developed on the REE pattern. Under environmental conditions, the most observed anomalies are the

Ce and Eu anomalies in response to biogeochemical processes. But non-conventional anomalies could also be expected for REE used as additive. For example, La stearate are largely used in PVC as heat stabilizer and could then produce non-conventional La anomaly on the REE pattern of plastics, exactly as what is obtained for Gd in the water receiving hospital effluents (Gd being used as contrast product for MRI examination) (Elbaz-Poulichet et al. 2002). Finally, before the application of this tracer method in complex environments, such as soils rich in OM or Fe/Mn oxyhydroxides, the impact of this third REE pool has to be evaluated (Davranche et al. 2015; Pourret et al. 2007). The present results demonstrate that in poor environments, such as beaches where REE sources are limited to few pools, REE can already trace the presence of NPs.

4. Conclusion

In the present study, we demonstrated the presence of nanoplastics in sand water extracts. Using DLS, TEM and Py-GCMS the identification of nanoplastics in the aqueous solution was validated. Analytical methodologies used here allows to size characterize and visualize the heterogeneity in size and shape of nanoplastics as well as the presence of other species that can be associated with (such as Iron oxide). PyGCMS appears to be adapted to identify NPs signature despite the abundancy of natural organic matter from Algae origin that can be found in beaches. While the NPs presence was expected due to the large quantity of microplastics observed and sampled on the beach, such identification could not give clear indication on their source and formation pathways. Marine sources of plastics on coast is the most probable due to the exposition of the beach to the oceanic current, however the contribution of in-situ contamination could also lead to specific incomes of plastic debris. Tracing NPs using geochemical approaches are therefore essential to better evaluate the environmental fate of plastic debris. To do so, we also explored the potential of rare earth elements (REE) in tracing nanoplastics. Based on the REE patterns of beached plastics and modern corals, we demonstrated that nanoplastics are important components in the REE signature of coastal sand (29 to 73%) and opens the door to new possibility for tracing such emerging contaminants. Further studies are dedicated to better evaluate the interaction mechanisms between NPs and REE and the implication of the NPs hetero-aggregation (natural organic matter, iron oxide, etc.). Geochemical approaches are urgently needed to raised up the challenge of the plastic debris tracing in the environment for developing mitigation plan.

CRediT authorship contribution statement

Mélanie Davranche: Conceptualization, Investigation, Methodology, Formal analysis, Validation. **Caroline Lory:** Investigation, Formal analysis. **Corentin Le Juge:** Investigation. **Florent Blancho:** Investigation. **Aline Dia:** Writing - review & editing. **Bruno Grassl:** Formal analysis. **Hind El Hadri:** Formal analysis. **Pierre-Yves Pascal:** Investigation. **Julien Gigault:** Conceptualization, Investigation, Methodology, Formal analysis, Validation, Funding acquisition, Project administration.

Declaration of Competing Interest

On the behalf of the authors, I certify that the authors of the manuscript entitled "Nanoplastics on the coast exposed to the North Atlantic Gyre: Evidence and traceability" have NO affiliations with or involvement in any organization or entity with any financial interest (such as honoraria; educational grants; participation in speakers' bureaus; membership, employment, consultancies, stock ownership, or other equity interest; and expert testimony or patent-licensing arrangements), or non-financial interest (such as personal or professional

Table 4
Proportion of coral sand and plastics as sources of REE for the < 0.8 μm fraction calculated by applying a mixing equation to the Eu anomaly, La/Sm ratio and Gd/Yb ratio with coral sand and plastics as both extremes.

	Eu anomaly (%)	La/Sm ratio (%)	Gd/Yb ratio (%)
Coral sand	71	54	27
Plastics	29	46	73

relationships, affiliations, knowledge or beliefs) in the subject matter or materials discussed in this manuscript.

Appendix A. Supplementary data

Supplementary data to this article can be found online at https://doi.org/10.1016/j.impact.2020.100262.

References

Andrady, A.L., 2011. Microplastics in the marine environment. Mar. Pollut. Bull. 62, 1596–1605. https://doi.org/10.1016/j.marpolbul.2011.05.030.

Balaram, V., 2019. Rare earth elements: a review of applications, occurrence, exploration, analysis, recycling, and environmental impact. Geosci. Front. 10, 1285–1303. https://doi.org/10.1016/j.gsf.2018.12.005.

Battistini, R., Hinschberger, F., 1985. La morphologie des côtes au vent de Grande-Terre et de Marie-Galante (Guadeloupe). (geomorphology of exposed shorelines of Grande-Terre and Marie-Galante - Guadeloupe.). Bulletin de l'Association de Géographes Français 62, 85–92. https://doi.org/10.3406/bagf.1985.1285.

Bau, M., 1999. Scavenging of dissolved yttrium and rare earths by precipitating iron oxyhydroxide: Experimental evidence for Ce oxidation, Y-Ho fractionation, and lanthanide tetrad effect. Geochimica et Cosmochimica Acta 63. doi:https://doi.org/10.1016/S0016-7037(99)00014-9.

Biller, P., Ross, A.B., 2014. Pyrolysis GC–MS as a novel analysis technique to determine the biochemical composition of microalgae. Algal Res. 6, 91–97. https://doi.org/10.1016/j.algal.2014.09.009.

Brennecke, D., Duarte, B., Paiva, F., Caçador, I., Canning-Clode, J., 2016. Microplastics as vector for heavy metal contamination from the marine environment. Estuar. Coast. Shelf Sci. 178, 189–195. https://doi.org/10.1016/j.ecss.2015.12.003.

Colton, J.B., Burns, B.R., Knapp, Frederick D., 1974. Plastic particles in surface waters of the northwestern Atlantic. Science 185, 491–497. https://doi.org/10.1126/science.185.4150.491.

Corti, A., Vinciguerra, V., Iannilli, V., Pietrelli, L., Manariti, A., Bianchi, S., Petri, A., Cifelli, M., Domenici, V., Castelvetro, V., 2020. Thorough multianalytical characterization and quantification of micro- and Nanoplastics from Bracciano Lake's sediments. Sustainability 12, 878. https://doi.org/10.3390/su12030878.

Cózar, A., Echevarría, F., González-Gordillo, J.I., Irigoien, X., Úbeda, B., Hernández-León, S., Palma, Á.T., Navarro, S., García-de-Lomas, J., Ruiz, A., Fernández-de-Puelles, M.L., Duarte, C.M., 2014. Plastic debris in the open ocean. PNAS 111, 10239–10244. https://doi.org/10.1073/pnas.1314705111.

Davranche, M., Gruau, G., Dia, A., Marsac, R., Pédrot, M., Pourret, O., 2015. Biogeochemical factors affecting rare earth element distribution in shallow wetland groundwater. Aquat. Geochem. 21, 197–215. https://doi.org/10.1007/s10498-014-9247-6.

Davranche, M., Veclin, C., Pierson-Wickmann, A.-C., El Hadri, H., Grassl, B., Rowenczyk, L., Dia, A., Ter Halle, A., Blancho, F., Reynaud, S., Gigault, J., 2019. Are nanoplastics able to bind significant amount of metals? The lead example. Environ. Pollut. 249, 940–948. https://doi.org/10.1016/j.envpol.2019.03.087.

Dignac, M.-F., Houot, S., Francou, C., Derenne, S., 2005. Pyrolytic study of compost and waste organic matter. Org. Geochem. 36, 1054–1071. https://doi.org/10.1016/j.orggeochem.2005.02.007.

El Hadri, H., Gigault, J., Maxit, B., Grassl, B., Reynaud, S., 2020. Nanoplastic from mechanically degraded primary and secondary microplastics for environmental assessments. NanoImpact 17, 100206. https://doi.org/10.1016/j.impact.2019.100206.

El Hadri, H., Gigault, J., Monicou, S., Grassl, B., Reynaud, S., 2021. Trace Element Distribution in Marine Microplastics Using Laser Ablation-ICP-MS. Marine Pollution Bulletin Article in press.

Elbaz-Poulichet, F., Seidel, J.-L., Othoniel, C., 2002. Occurrence of an anthropogenic gadolinium anomaly in river and coastal waters of southern France. Water Res. 36, 1102–1105. https://doi.org/10.1016/S0043-1354(01)00370-0.

Fabbri, D., Trombini, C., Vassura, I., 1998. Analysis of polystyrene in polluted sediments by pyrolysis—gas chromatography—mass spectrometry. J. Chromatogr. Sci. 36, 600–604.

Fu, W., Min, J., Jiang, W., Li, Y., Zhang, W., 2020. Separation, characterization and identification of microplastics and nanoplastics in the environment. Sci. Total Environ. 721, 137561. https://doi.org/10.1016/j.scitotenv.2020.137561.

Geyer, R., Jambeck, J.R., Law, K.L., 2017. Production, use, and fate of all plastics ever made. Sci. Adv. 3, e1700782. https://doi.org/10.1126/sciadv.1700782.

Gigault, J., Pedrono, B., Maxit, B., Halle, A.T., 2016. Marine plastic litter: the unanalyzed nano-fraction. Environ. Sci.: Nano 3, 346–350.

Gigault, J., El Hadri, H., Reynaud, S., Deniau, E., Grassl, B., 2017. Asymmetrical flow field flow fractionation methods to characterize submicron particles: application to carbon-based aggregates and nanoplastics. Anal. Bioanal. Chem. 409, 6761–6769. https://doi.org/10.1007/s00216-017-0629-7.

Gigault, J., Ter Halle, A., Baudrimont, M., Pascal, P.-Y., Gauffre, F., Hadri, H.E., Grassl, B., Reynaud, S., 2018. Current opinion: what is a nanoplastic? Environ. Pollut. 235, 1030–1034.

Holmes, L.A., Turner, A., Thompson, R.C., 2012. Adsorption of trace metals to plastic resin pellets in the marine environment. Environ. Pollut. 160, 42–48. https://doi.org/10.1016/j.envpol.2011.08.052.

Howell, E.A., Bograd, S.J., Morishige, C., Seki, M.P., Polovina, J.J., 2012. On North Pacific circulation and associated marine debris concentration. Mar. Pollut. Bull. 65, 16–22. https://doi.org/10.1016/j.marpolbul.2011.04.034.

Jambeck, J.R., Geyer, R., Wilcox, C., Siegler, T.R., Perryman, M., Andrady, A., Narayan, R., Law, K.L., 2015. Plastic waste inputs from land into the ocean. Science 347, 768–771. https://doi.org/10.1126/science.1260352.

Kusch, P., 2012. Pyrolysis-Gas Chromatography/Mass Spectrometry of Polymeric Materials. https://doi.org/10.5772/32323.

Maris, E., Aoussat, A., Naffrechoux, E., Froelich, D., 2012. Polymer tracer detection systems with UV fluorescence spectrometry to improve product recyclability. Minerals Engineering, Sustainability through Resource Conservation and Recycling 29, 77–88. https://doi.org/10.1016/j.mineng.2011.09.016.

McLennan, S.M., 1989. Rare earth elements in sedimentary rocks; influence of provenance and sedimentary processes. Rev. Mineral. Geochem. 21, 169–200.

Mintenig, S.M., Bäuerlein, P.S., Koelmans, A.A., Dekker, S.C., Van Wezel, A.P., 2018. Closing the gap between small and smaller: towards a framework to analyse nano- and microplastics in aqueous environmental samples. Environmental Science: Nano 5, 1640–1649. https://doi.org/10.1039/c8en00186c.

Nelms, S.M., 2009. Inductively Coupled Plasma Mass Spectrometry Handbook.

Ohta, A., Kawabe, I., 2001. REE(III) adsorption onto Mn dioxide (δ-MnO2) and Fe oxyhydroxide: Ce(III) oxidation by δ-MnO2. Geochim. Cosmochim. Acta 65, 695–703. https://doi.org/10.1016/S0016-7037(00)00578-0.

Pourret, O., Davranche, M., Gruau, G., Dia, A., 2007. Rare earth elements complexation with humic acid. Chem. Geol. 243, 128–141. https://doi.org/10.1016/j.chemgeo.2007.05.018.

Prunier, J., Maurice, L., Perez, E., Gigault, J., Pierson Wickmann, A.-C., Davranche, M., Halle, A.T., 2018. Trace metals in polyethylene debris from the North Atlantic subtropical gyre. Environ. Pollut. 245, 371–379. https://doi.org/10.1016/j.envpol.2018.10.043.

Rouches, E., Dignac, M.-F., Zhou, S., Carrere, H., 2017. Pyrolysis-GC–MS to assess the fungal pretreatment efficiency for wheat straw anaerobic digestion. J. Anal. Appl. Pyrolysis 123, 409–418. https://doi.org/10.1016/j.jaap.2016.10.012.

Schmidt, C., Krauth, T., Wagner, S., 2017. Export of plastic debris by Rivers into the sea. Environ. Sci. Technol. 51, 12246–12253. https://doi.org/10.1021/acs.est.7b02368.

Schwaferts, C., Niessner, R., Elsner, M., Ivleva, N.P., 2019. Methods for the analysis of submicrometer- and nanoplastic particles in the environment. TrAC Trends Anal. Chem. 112, 52–65. https://doi.org/10.1016/j.trac.2018.12.014.

Shim, W.J., Song, Y.K., Hong, S.H., Jang, M., Han, G.M., Jung, S.W., 2014. Producing fragmented micro-and nano-sized expanded polystyrene particles with an accelerated mechanical abrasion experiment. In: 24th Europe SETAC annual meeting, Basel, Switzerland, pp. 11–15.

Sholkovitz, E., Shen, G.T., 1995. The incorporation of rare earth elements in modern coral. Geochim. Cosmochim. Acta 59, 2749–2756. https://doi.org/10.1016/0016-7037(95)00170-5.

Ter Halle, A., Jeanneau, L., Martignac, M., Jardé, E., Pedrono, B., Brach, L., Gigault, J., 2017. Nanoplastic in the North Atlantic subtropical gyre. Environ. Sci. Technol. 51, 13689–13697. https://doi.org/10.1021/acs.est.7b03667.

Wahl, A., Davranche, M., Grassl, B., El Hadri, H., Gigault, J., 2020. Nanoplastics Occurence in an Amended Soil. (Journal of Hazardous Materials Article submitted).

Wahl, A., Le Juge, C., Davranche, M., El Hadri, H., Grassl, B., Reynaud, S., Gigault, J., 2021. Nanoplastic occurrence in a soil amended with plastic debris. Chemosphere 262, 127784. https://doi.org/10.1016/j.chemosphere.2020.127784.

Watteau, F., Dignac, M.-F., Bouchard, A., Revallier, A., Houot, S., 2018. Microplastic Detection in Soil Amended With Municipal Solid Waste Composts as Revealed by Transmission Electronic Microscopy and Pyrolysis/GC/MS. Front. Sustain. Food Syst. 2. https://doi.org/10.3389/fsufs.2018.00081.

Zbyszewski, M., Corcoran, P.L., Hockin, A., 2014. Comparison of the distribution and degradation of plastic debris along shorelines of the Great Lakes, North America. J. Great Lakes Res. 40, 288–299. https://doi.org/10.1016/j.jglr.2014.02.012.